MEASUREMENT AND PREDICTION OF LEAKAGE AND CAVITY PRESSURES IN A 0.3 MM CLEARANCE INTERLOCKING LABYRINTH SEAL WITH THREE SWIRL BRAKE DESIGNS

Luis San Andrés	**Jing Yang**	**Rimpei Kawashita**
Mast-Childs Chair Professor	Research Associate	Research Engineer
lsanandres@tamu.edu	yangjing@tamu.edu	rinpei_kawashita@mhi.co.jp

J. Mike Walker '66 Department of Mechanical Engineering, Texas A&M University   Mitsubishi Heavy Industries, Ltd.

ABSTRACT

By reducing secondary leakage in turbomachinery, gas labyrinth seals (LSs) improve their operational efficiency and mechanical reliability. As interlocking labyrinth seals (ILSs) restrict more leakage than conventional see-through LSs, attention is due to their performance. The paper details the performance of a particular ILS geometry via measurements of mass flow (leakage) and cavity pressures in an ad-hoc test rig operating with pressurized air at ambient temperature. The seal comprises of two teeth on the rotor and three teeth on the stator to make a four cavity seal with radial clearance $C_r = 0.3$ mm. The ILS is first configured without a swirl brake (baseline), next with a swirl brake with 0° teeth pitch (axial ribs), and last with a swirl brake with teeth angled at 40° in the direction of shaft rotation. During the tests conducted without shaft rotation and with rotor spinning at 7.5 krpm (surface speed= 59 m/s), the inlet air pressure (P_{in}) ranges from 0.29 MPa to 0.98 MPa, while the exit pressure (P_{out}) is set to a desired pressure ratio $PR = (P_{out}/P_{in}) = 0.3, 0.5, 0.8$. The measurements and computational physics predictions show that the seals' mass leakage is proportional to the inlet pressure (P_{in}), increases as PR decreases, and is not affected by either shaft speed or the swirl brake configuration. Seal cavity static pressures drop linearly for all inlet pressures (P_{in}) and PR=0.5 and 0.8; except under choked conditions at $PR = 0.3$. Processing of the test data to consolidate the numerous leakage measurements delivers a nearly invariant flow factor $\bar{\Phi}$, and from this follows a unique seal loss coefficient c_d =0.36. This finding is remarkable as it also applies to test results obtained with a similar ILS, 0.2 mm clearance, as published earlier [1]. Finally, predictions of ILS leakage are within 5% of the measurements for all test conditions. The test data and predictions are of significant value to better the selection and design of gas labyrinth seals in turbomachinery.

INTRODUCTION

Labyrinth seals (LSs), mechanical components reducing secondary leakage flow, find wide application in compressors and steam turbines. Depending on the tooth configuration, there are several kinds of LSs, such as a see-through LS, an interlocking labyrinth seal (ILS), and a stepped LS. See-through LSs include the tooth-on-rotor (TOR) and tooth-on-stator (TOS) types, whereas an ILS has teeth on both the rotor and stator surfaces. The stepped LSs have steps both on the rotor and the stator. The tortuous flow path in a LS induces a pressure drop (a loss of energy) and as it controls the leakage.

There are already plenty of experimental investigations reporting the leakage characteristics and dynamic force performance for both TOR and TOS LSs [2], although few experimental results are found for ILSs. As early as in 1980, Benkert and Wachter [3] measure the lateral force component for a series of LSs (TOR, TOS, interlocking, and stepped LSs) for various inlet pre-swirl conditions. The experimental results show the inlet circumferential pre-swirl has a negative effect on rotor stability, whereas a swirl brake at the seal inlet reduces the magnitude of the seal cross-coupled stiffness coefficient. In 1988, Childs et al. [4] measure the leakage and dynamic force coefficients for a TOS LS and an ILS operating with maximum supply pressure equal to 8 bar and at a rotor speed ranging from 3 krpm to 16 krpm (surface speed 47 m/s to 251 m/s). These two LSs have comparable physical dimensions. The leakage of the ILS is much lesser than that in the TOS LS. Though having a direct damping coefficient only equal to 50% of that for the TOS LS, the ILS shows a smaller (negative) cross-coupled stiffness. Thus the test ILS has a lower whirl frequency ratio, indicating better performance for rotor stability.

In 2007, Paolillo et al. [5] investigate the impact of rotational shaft speed on seal leakage for various stepped LSs. The test data indicate the ratio between the rotor surface speed and axial flow velocity has a significant influence on the seal leakage. In 2011, Bozzi et. al. [6] employ a stationary test rig to evaluate the effects of seal clearance on the leakage flow and heat transfer coefficients for a particular LS used in a heavy-duty gas turbine. The test data for this type of LS show a derived flow factor[1] (ϕ) does not linearly depend on the seal clearance.

---

[1] The flow factor characterizes a seal leakage independently of its diameter and inlet flow conditions (supply pressure and temperature).

In 2014, Vannini et al. [7] introduce a test apparatus for high pressure gas seals and report the dynamic force coefficients for a TOS LS operating with both a highly positive and negative inlet pre-swirl ratio[2] (± 0.9). The test data show the inlet pre-swirl velocity has a dramatic impact on the seal cross-coupled stiffness coefficients, whereas its influence on the direct stiffness and direct damping coefficients is relatively low.

In 2016, Childs et al. [8] conduct experiments with a sixteen teeth TOS LSs; one seal without swirl brake, another seal with a conventional (straight radial rib) swirl brake, and a third seal with a negative swirl brake. The test results demonstrate the LS operating with a well-designed negative swirl brake leaks ~ 9% less than the seal without a swirl brake. The straight swirl brake induces a 20% drop in the seal cross-coupled stiffness coefficient in comparison to that for the LS without a swirl brake. The negative swirl brake changes the value of the seal cross-coupled stiffness into a negative number. The LS operating with a negative swirl brake also has a remarkable increase of its effective damping in comparison to that for the seal without a swirl brake.

Later in 2018, Gary et al. [9] introduce a gas seal test rig and measure the leakage and dynamic force coefficients for an ILS operating with and without a swirl brake. The seal clearance $C_r = 0.2$ mm. The supply pressure ranges from 2.75 bar towards 4.83 bar and the rotor speed equals to 10 krpm (surface speed 79 m/s). The test rig failed to produce reliable data for leakage and dynamic force coefficients due to several technical issues. In 2019, San Andrés et al. [1] revamp the test rig and report the experimental and numerical leakages for an ILS without swirl brake operating with various supply pressures and rotor speeds. The authors note that rotor speed has a minute effect on the seal leakage flow; and find the measured leakage and predicted leakage agree well.

Bulk-flow model (BFM) and computational fluid dynamics (CFD) are two common numerical tools to predict the performance of LSs. The BFM is a time efficient method, though not as accurate as CFD is. Most BFMs select Neumann's equation [10] to predict the seal leakage and cavity pressures, including one developed by Thorat and Childs [11] that is widely used in industry.

As a follow-up research on the experimental and numerical investigations on an ILS [1], this paper details the measurements of leakage for an ILS with a large clearance ($C_r = 0.3$ mm), operating with no swirl brake (baseline), with a swirl brake having 0° teeth pitch (radial ribs), and with a swirl brake having 40° (angle in flow direction) teeth pitch. The BFM [11] predicted seal leakage and cavity pressures follow closely the test data.

A BRIEF NOTE ON PREDICTING LEAKAGE

Figure 1 shows on the left a typical cross-section view for a five teeth ILS; three teeth on the stator and two teeth on the rotor create four cavities. Gas at inlet pressure (P_{in}) and temperature (T) flows through the LS teeth with radial clearance (C_r) and exits at pressure (P_{out}). The graph on the right depicts a single tooth seal whose intent is to represent the actual seal with an effective clearance (C_{eff}) and having the same leakage.
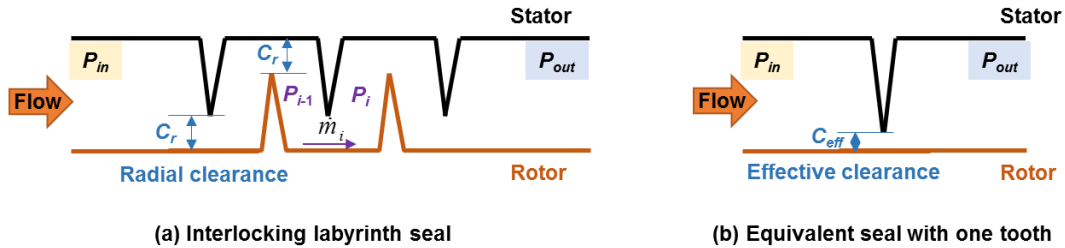

(a) Interlocking labyrinth seal   (b) Equivalent seal with one tooth

Figure 1. Schematic views of (a) an interlocking labyrinth seal and (b) an equivalent single-tooth seal with effective clearance (C_{eff}).

Typically modeled with Neumann's equation [10], the mass flow rate ($\dot{m}_i$) under the ith tooth is a function of the upstream cavity pressure (P_{i-1}), the downstream cavity pressure (P_i) and the restriction area with clearance (C_r) and shaft diameter D. This leakage equals

$$\dot{m}_i = \mu_{1i}\mu_{2i}(\pi D C_r)\sqrt{\frac{P_{i-1}^{\,2} - P_i^2}{R_g T}} \,, i = 1, 2 \ldots N_T \tag{1}$$

---

[2] The inlet pre-swirl ratio equals to the inlet circumferential velocity divided by the rotor surface speed (ΩR). Typical swirl ratios equaling to 0.5 and above are not desired.

where μ_{1i} is a kinetic energy carry-over coefficient and μ_{2i} is a flow discharge coefficient, both functions of the seal geometry, number of teeth N_T, and pressure ratio $PR = P_{out}/P_{in}$. [10]. Recall that for an ideal gas its density $\rho = P/(R_g T)$ where R_g is the gas constant.

For a seal with uniform flow restriction area ($\pi D\, C_r$), the mass flow rate under a tooth is a constant, i.e., $\dot{m}_1 = \dot{m}_2 = ... = \dot{m}$; hence

$$P_{in}^{\,2} - P_1^2 = \frac{1}{(\mu_{11}\mu_{21})^2}\left[\frac{\dot{m}\sqrt{R_g T}}{\pi DC_r}\right]^2$$

$$P_1^2 - P_2^2 = \frac{1}{(\mu_{12}\mu_{22})^2}\left[\frac{\dot{m}\sqrt{R_g T}}{\pi DC_r}\right]^2 \quad ;$$

$$...$$

$$P_{N_T}^2 - P_{out}^{\,2} = \frac{1}{(\mu_{12}\mu_{22})^2}\left[\frac{\dot{m}\sqrt{R_g T}}{\pi DC_r}\right]^2$$

(2)

Summing all the equations above gives

$$P_{in}^{\,2} - P_{out}^{\,2} = \frac{1}{c_d^{\,2}}\left[\frac{\dot{m}\sqrt{R_g T}}{\pi DC_r}\right]^2 \quad \text{with} \quad \frac{1}{c_d^{\,2}} = \sum_{i=1}^{N_c}\frac{1}{\mu_{1i}\mu_{2i}}$$

(3)

Therefore, the seal leakage is written as

$$\dot{m} = c_d(\pi DC_r)P_{in}\sqrt{\frac{1 - PR^2}{R_g T}}$$

(4)

where c_d stands for a seal (orifice-like) loss coefficient and the product ($c_d\, C_r$) is understood as the effective clearance (C_{eff}) of the single tooth seal equivalent to the physical multiple-teeth seal.

In 2006, Delgado and Proctor [12] introduced the seal flow factor $\phi = \dot{m}\sqrt{T}\big/DP_{in}$, which is used extensively to characterize and to compare the leakage behavior of many distinct a seal. Alas this flow factor has unusual physical units $[^{kg}\!\!/_{s}\sqrt{K}/(MPa\,m)]$ and does not relate to the exit pressure P_{out}. A more realistic modified flow factor developed in Ref. [1] is

$$\bar{\Phi} = \frac{\dot{m}\sqrt{T}}{P_{in}D\sqrt{1 - PR^2}} = \pi\frac{C_{eff}}{\sqrt{R_g}}$$

(5)

Note that the right side of Eq. (5) relates the flow factor to the effective clearance (C_{eff}) and the gas composition (R_g). For a test ILS with clearance $C_r=0.2$ mm, San Andrés et al. [1] find $c_d = 0.3$ and thus a constant $\bar{\Phi}$, irrespective of operating conditions; namely inlet and exit pressures and rotor speed.

DESCRIPTION OF THE TEST RIG

Figure 2 shows a photograph of the test rig for gas seals and comprising the drive motor section, the test rotor and its supports, and the test seal and housing section. The driver includes a drive motor, a belt pulley system for speed increase, a quill shaft, and an emergency brake system (not shown in Figure 2). A pair of magnetic bearings support a steel rotor at its two ends. The steel rotor is 100 mm in diameter, 1.6 m long and weighing 980 N. The test seal section comprises two seals adjacent to a center plenum for pressurized air delivery, as well as the instrumentation and the locations of both the inlet and outlet pressure sensors, eddy current displacement sensors facing the rotor, and a pitot tube for measurement of the inlet swirl velocity. Ref. [1] provides further details on the test rig.
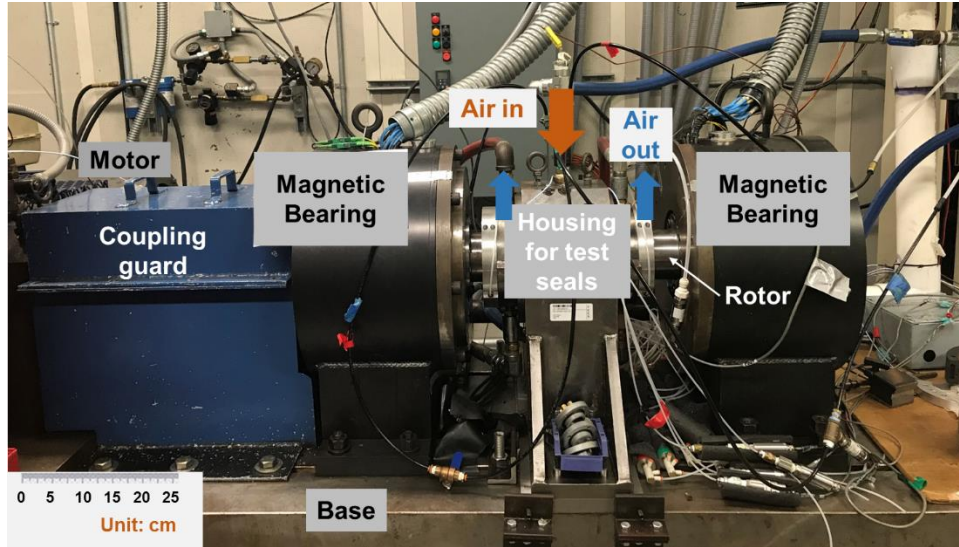
Figure 2. Photograph of test rig for gas seals.

Error! Reference source not found. shows a cross-section view of the ILS teeth profile with dimensions noted, and Table 1 lists the seal geometry and operating conditions. The ILS has three teeth on the stator and two teeth on the rotor to create four cavities. Note all teeth have the same dimensions and a nominal seal radial clearance $C_r = 0.3 \pm 0.013$ mm[3]. As air flows through the cavities, four pressure transducers collect the static pressure (P_{cav}) in each cavity, as depicted in **Error! Reference source not found.** (one sensor per cavity).

Table 1 . Seal geometry and operating conditions.

Seal Geometry	Rotor diameter, D	150 mm
	Overall length, L	45 mm
	Radial clearance, C_r	300 µm
	Teeth Number, NT	5
	Tooth Pitch, L_i	8.3 mm
	Height, B	5.8 mm
	Width at tip, B_t	0.25 mm
Air Properties	Density, ρ @ 25˚C	1.2 kg/m^3
	Temperature, T	298 K
	Sound speed, V_s	350 ~ 354 m/s
	Kinematic viscosity, v	1.86×10^{-5} m^2/s
Operating Conditions	Supply pressure P_s	0.79 ~ 1.83 MPa
	Inlet Pressure, P_{in}	0.29 ~ 0.98 MPa
	Pressure ratio, $PR = P_{out}/P_{in}$	0.3, 0.5, 0.8
	Rotor speed, Ω	0, 3, 5, 7.5 krpm
	Surface Speed, $R\Omega$	0 ~ 59 m/s

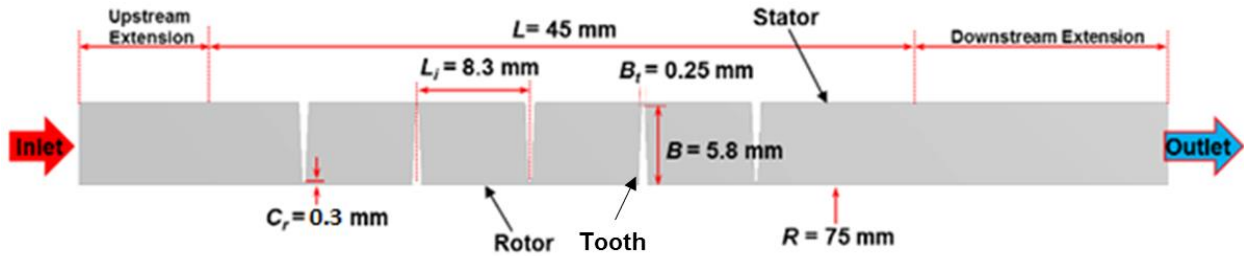[3] A prior seal in Ref. [1], similar in construction, has radial clearance $C_r = 0.2$ mm.

Figure 3. Schematic planar view of ILS test configuration.

A 2.17 MPa maximum rated compressor system provides pressurized air to the test section, shown in Figure 5. A flow meter and pressure sensor, installed 10 meter upstream from the test section, measure the air volumetric flow rate ($\dot{Q}$) and the static pressure in the supply line (P_{line}), respectively. A central section is installed midway between two aluminum test seals, see Figure 4, left and right. The central section assembly comprises three parts; (a) a middle or central ring with angled orifices for the supply of air and to create inlet swirl in the direction or rotor spinning, (b) a ridge or bridge isolating the seals (left and right) from the inlet air supply plenum, and (c) swirl brakes for inducing inlet swirl flow and routing the gas in a certain direction, see **Error! Reference source not found.** and 5. An additive manufacturing process known as Fused Deposition Modeling (FDM), or Fused Filament Fabrication (FFF) makes each of the three central section components, which are made of polylactic acid (PLA) material.

Table 2 lists the components of the central section assembly next to the left and right seals while Figure 6(a) depicts a schematic view with details on the flow path from a feed hole, crossing a bridge and into the swirl brake just before a seal inlet plane. There are three seal configurations, displayed in Figure 7, (1) one mid ring with no swirl brake (baseline swirl), (2) another with a swirl brake with 0° teeth pitch (axial ribs), and (3) a third mid ring with a swirl brake with ribs angled at 40° in the direction of rotation.

Note the mid ring geometry is the same for all seal configurations, having two rows of 14 inlet orifices, each 1.5 mm in diameter, and 75° away from the radial direction, see Figure 6(b). Note the holes disposition injects pressurized air into the central plenum in the same direction as the rotor spins.
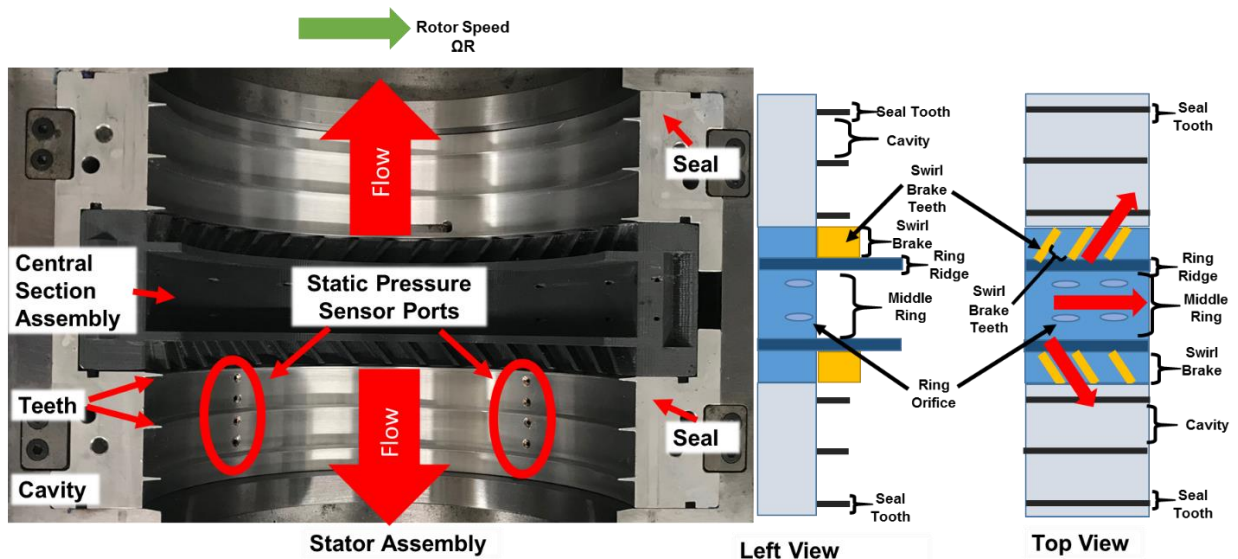

Figure 4. Photograph and schematic view of a half seal assembly with location of pressure sensors in seal cavities.
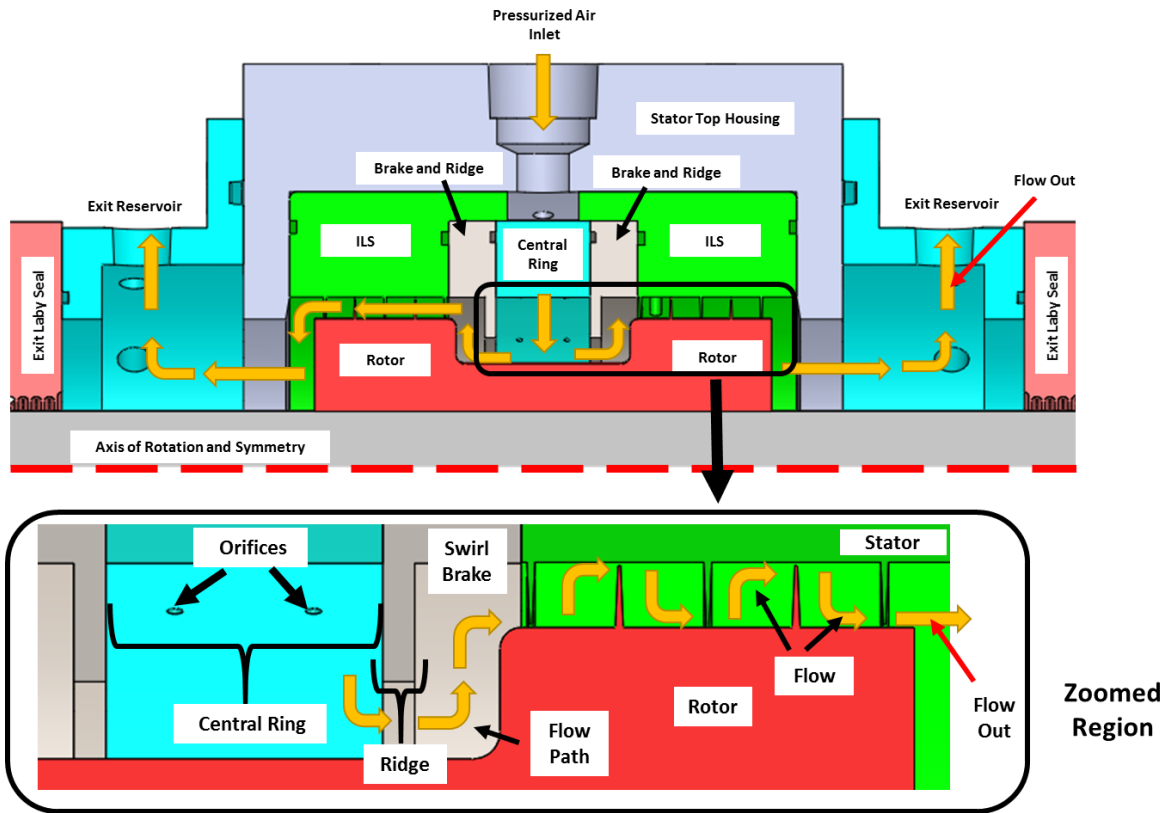
5

Figure 5. Axial cross section of complete housing and seals assembly with flow path details. Zoomed section shows a close up of the flow path on the instrumented seal.

**Table 2. Geometry of mid ring and a swirl brake***

|		
	Swirl direction	+ pre-swirl (With rotor rotation)
	Ring ridge height (a)	11.1 mm
	Ring ridge thickness (b)	3 mm
Central Ring Description	Mid ring width ©	26 mm
	Mid ring ID (d)	162 mm
	Ring OD ©	204 mm
	Orifice number	28
	Orifice inlet angle (f)	75˚
	Orifice diameter (g)	1.5 mm
	Teeth number	34 (equally spaced)
	width (h)	10 mm
Swirl Brake Description	Height (i)	5.4 mm
	Tooth thickness (j)	2 mm
	ID (k)	162 mm
	Axial rib pitch (l)	**Brake #1: 0˚; Brake #2: 40˚

*See Figure 6 (a) and Figure 6 (b).
**Brake #1 is the teeth pitch for central ring assembly 2, and Brake #2 is the teeth pitch for central ring assembly 3.

Figure 7 portrays photographs of the three test seal configurations. In the graphs, the red arrows denote the direction of the inlet air as it enters the plenum and the air flow path through the swirl brake and ILS, whereas the

green arrow denotes the direction of rotor spinning. The pitch of the axial ribs is the only difference between the two swirl brake geometries in the central section for assemblies 2 and 3. Otherwise, all other dimensions are the same.
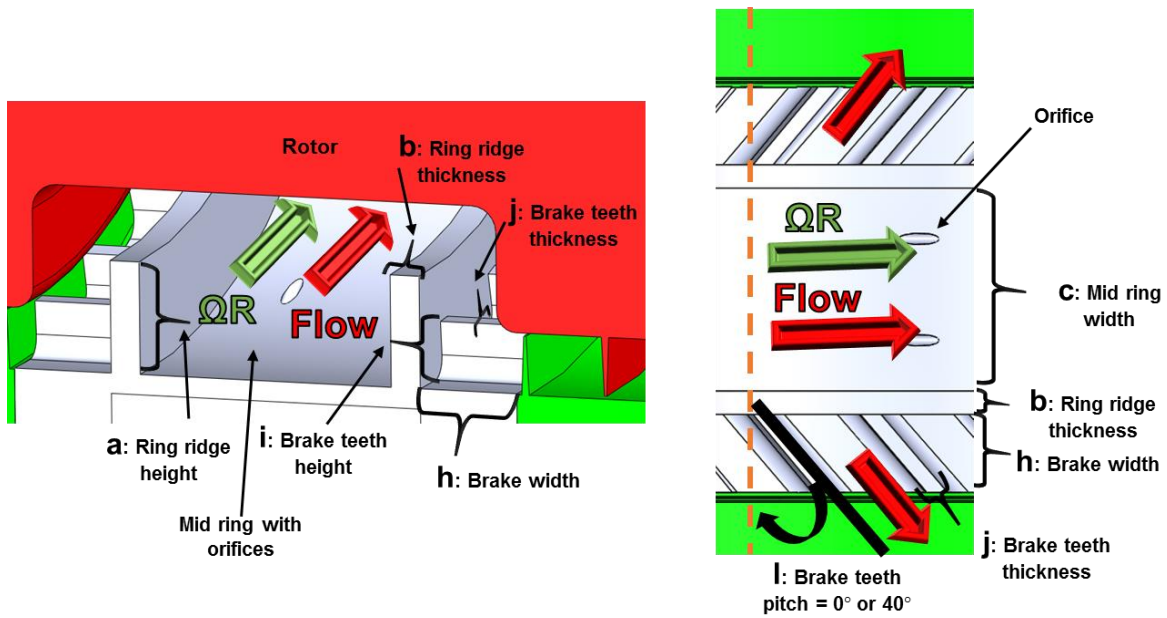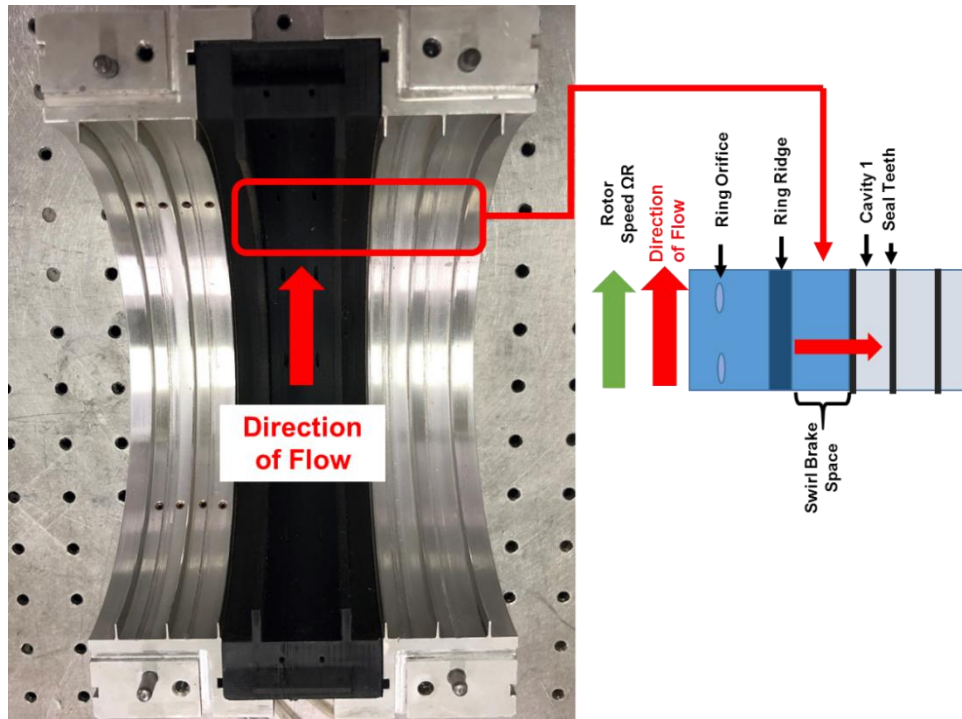

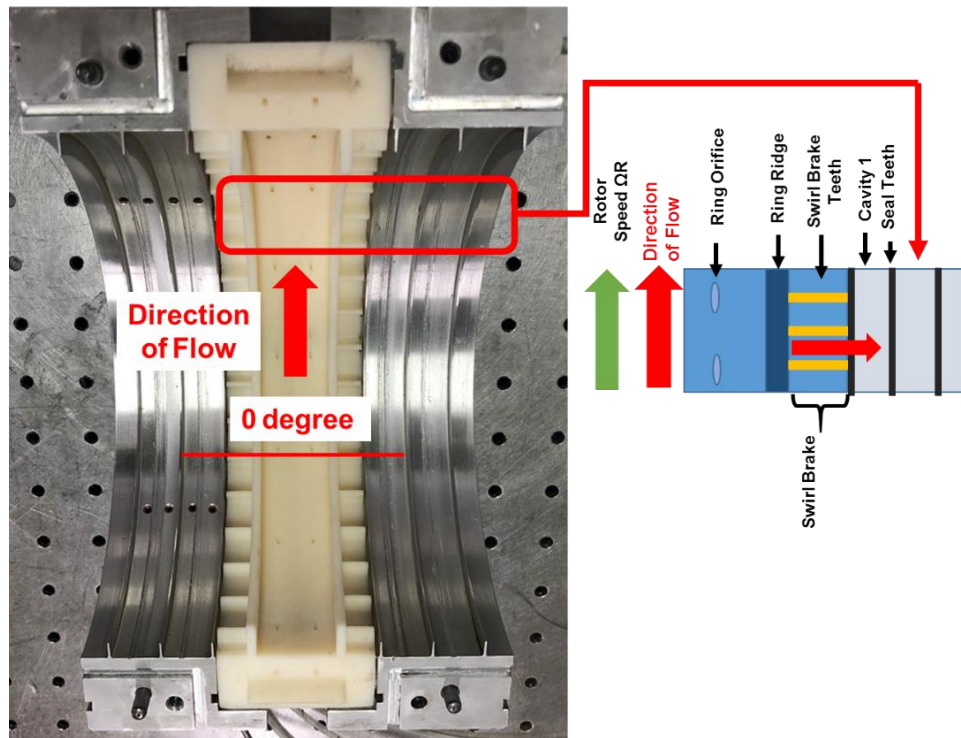**(a) Central section assembly cross-section view with geometry details.**
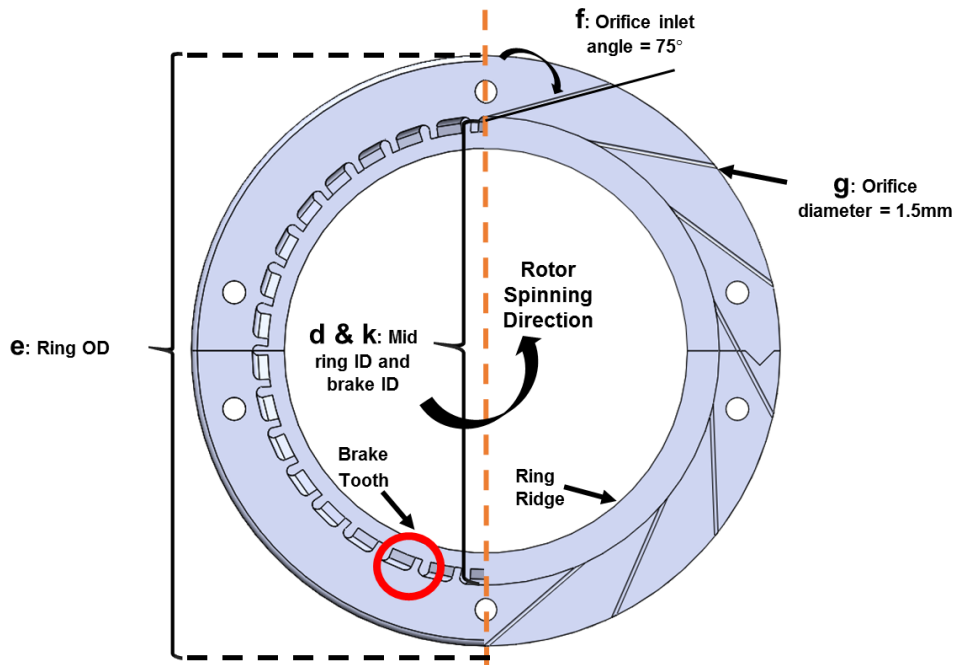
(b) Mid ring with angled injection holes.

Figure 6. Schematic views of (a) central section assembly and (b) mid ring with holes.
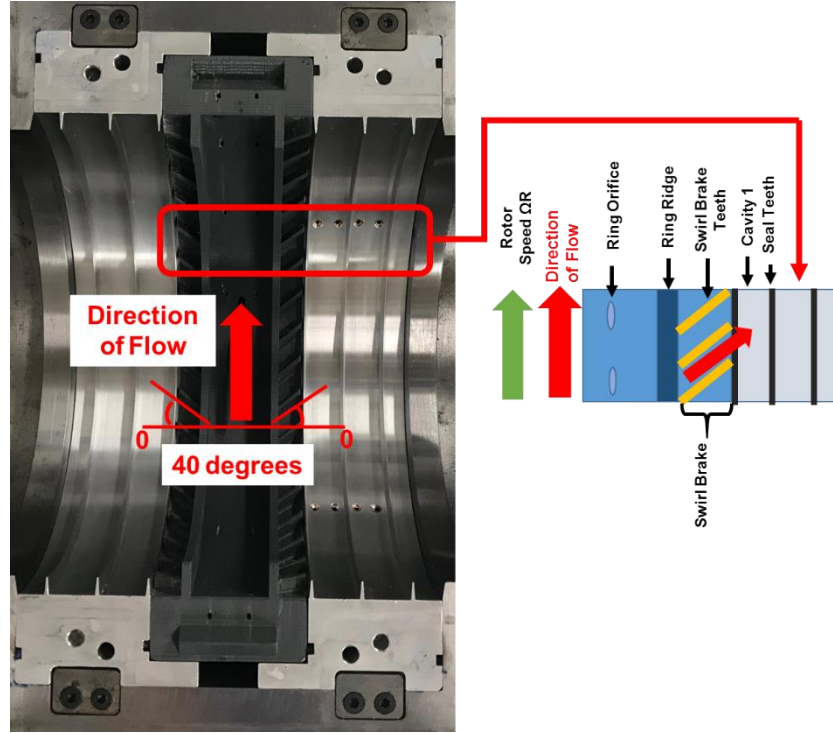
(a) Test seal assembly with no swirl brake.

(b) Test seal assembly with swirl brake, 0° teeth pitch

Figure 7. Photographs and cross-sectional views of test seal section with (a) no swirl brake, (b) swirl brake with 0° teeth pitch, and (c) swirl brake with 40° teeth pitch.

(c) Test seal assembly with swirl brake, 40° teeth pitch in the direction of rotation.

Figure 7 (continued). Photographs and cross-sectional views of test seal section with (a) no swirl brake, (b) swirl brake with 0° teeth pitch, and (c) swirl brake with 40° teeth pitch.

EXPERIMENTAL RESULTS AND DISCUSSION

The three ILS with distinct swirl brake configurations shown in Figure 7 are supplied with pressurized air ambient temperature T_{in}= 295~305 K. The air inlet pressure P_{in}, ranging from 0.29 MPa to 0.98 MPa, is recorded just upstream of the ILS inlet plane. A throttle valve regulates the discharge reservoir pressure P_{out} and sets the pressure ratio $PR = (P_{out}/P_{in}) = 0.3$, 0.5, and 0.8. During the tests, the rotor speed is set at 0, 3 krpm, 5 krpm and 7.5 krpm (max. surface speed $R\Omega = 59$ m/s) albeit experimental results for operation at 0 rpm and 7.5 krpm are hereby presented.

Prior work with the current ILS in Ref. [1] already establishes that rotor speed has a minimal effect on ILS leakage and cavity pressures. For example, a 4% maximum difference is typical for the current test results against those obtained with rotor speeds equaling 3 krpm and 5 krpm for all PRs [1].

For the current test seal configurations, the operation allows for a limited range of inlet pressure (P_{in}) with a set pressure ratio PR. That is, at pressure ratio $PR = 0.3$, P_{in} ranges from 0.5 to 0.7 MPa, whereas for $PR = 0.5$, P_{in} varies from 0.25 to 0.74 MPa, and for $PR = 0.8$, P_{in} ranges from 0.13 to 1.03 MPa.

Gas inlet swirl velocity for test ILS

The inlet or supplied swirl velocity $U_{swirl} \sim \sqrt{2\,\Delta P_{piv}/\rho_{in}}$ at the feed plenum underneath the mid ring is a function of the pressure difference ΔP_{piv} = (static - dynamic) collected by a differential pressure sensor, via a pitot tube, and the local density (ρ_{in}) [1]. Note that this gas inlet swirl velocity[4] is at the mid plane of the central section assembly and in the direction of rotor spin. A constant $P_{in} \sim 0.60$ MPa provides a means for comparing the inlet gas swirl velocity across all PR.

For the baseline seal assembly (without a swirl brake), Figure 8(a) shows that the inlet gas swirl velocity (U_{swirl}) ranges from 151 m/s ($PR = 0.8$, P_{in} =0.60 MPa) to 223 m/s ($PR = 0.3$, P_{in} =0.60 MPa) for both operating rotor speeds,

---

[4] The velocity hereby presented is that just downstream of the supply holes and (likely very) different from the swirl velocity of the gas entering the ILS.

0 and 7.5 krpm. The hollow symbols represent U_{swirl} at null rotor speed, whereas the solid symbols denote U_{swirl} at 7.5 krpm ($R\Omega = 59$ m/s). Triangle, diamond, and circle symbols denote the test data at pressure ratio $PR = 0.3$, 0.5, and 0.8, respectively. At $P_{in} = 0.59$ MPa, the second seal configuration with swirl brakes having 0° teeth pitch (axial ribs) shows $U_{swirl} = 133$ m/s at $PR = 0.8$ and 191 m/s at $PR = 0.3$, see Figure 8(b). The difference in U_{swirl} with that for the baseline configuration is ~ 15% reduction. In Figure 8(c), at $P_{in} = 0.60$ MPa, the seal with a swirl brake having 40° axial ribs (in the direction of shaft rotation) shows $U_{swirl} = 111$ m/s at $PR = 0.8$ and 158 m/s at $PR = 0.3$. The difference with U_{swirl} for the baseline configuration is ~ 30% decrease. Thus, the addition of the swirl brakes affects U_{swirl} at the feed plenum, likely due the addition of a flow resistance when the gas travels through the ribs, when angled in particular. Recall U_{swirl} is in the direction of shaft speed albeit shaft speed does not affect it. Incidentally, the recorded U_{swirl} tells nothing about the actual circumferential swirl velocity at the entrance plane of the ILS.
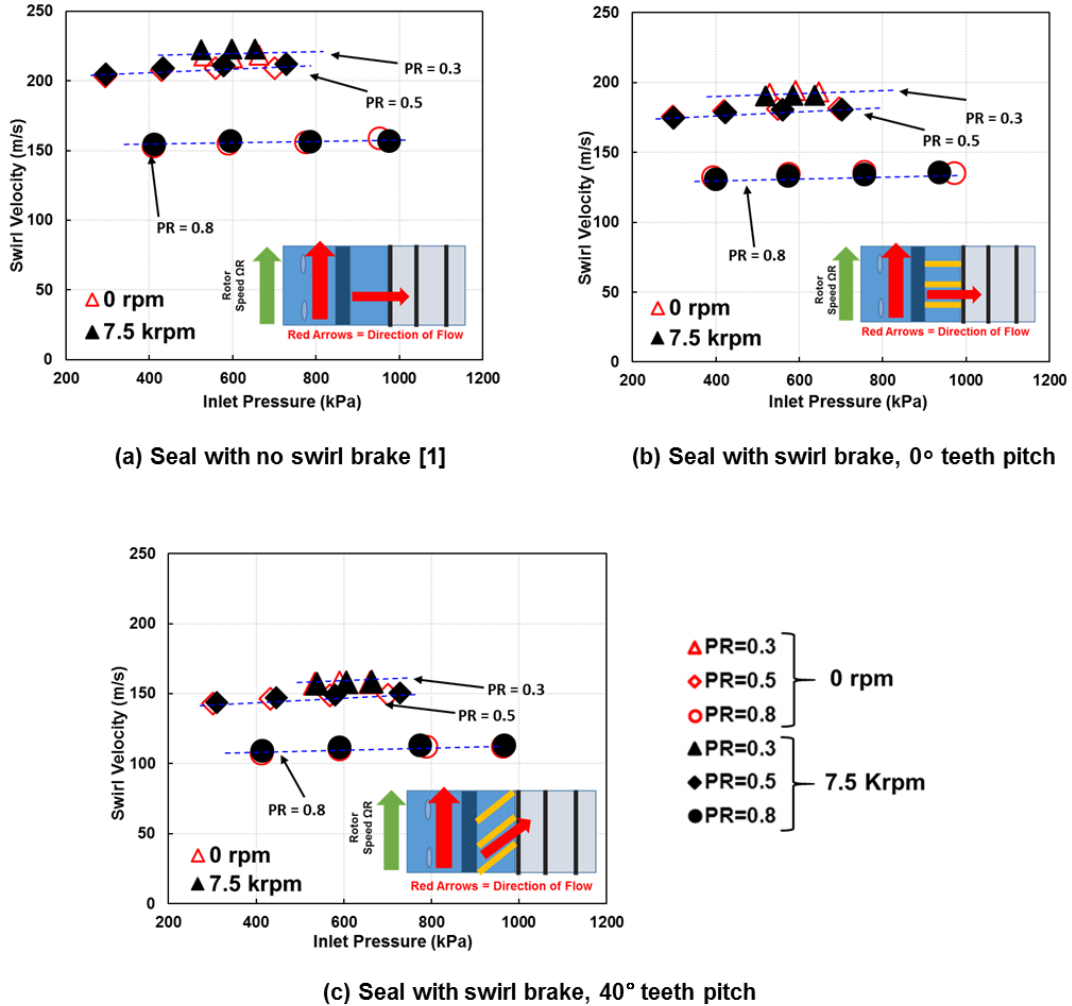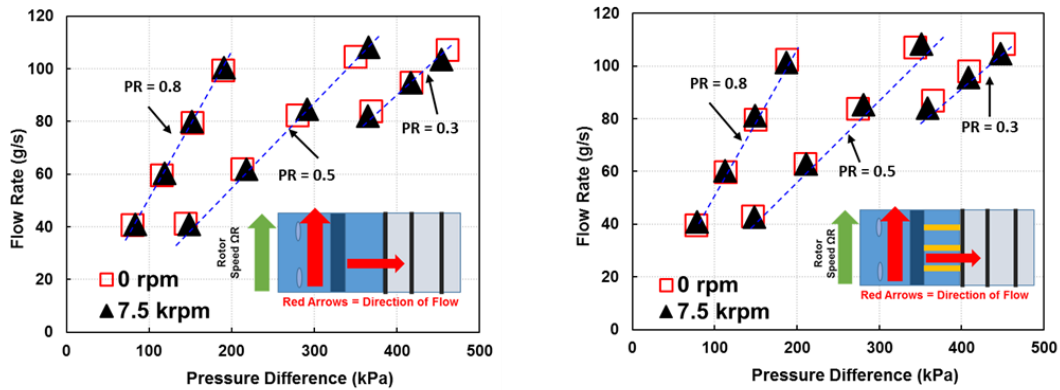

(a) Seal with no swirl brake [1]

(b) Seal with swirl brake, 0° teeth pitch

(c) Seal with swirl brake, 40° teeth pitch

Figure 8. Plenum inlet gas swirl velocity (Uswirl) versus inlet pressure P_{in} for three test seal configurations: (a) no swirl brake, (b) swirl brake with 0° teeth pitch, and (c) swirl brake with 40° teeth pitch. ILS operates at three pressure ratios (PR = 0.3, 0.5, 0.8) and two rotor speeds (Ω =0, 7.5 krpm, max $R\Omega$ = 59 m/s).

Mass flow rate for test ILS

Figure 9 depicts the measured mass flow rate ($\dot{m}$) for each ILS configuration versus pressure difference $\Delta P = (P_{in} - P_{out})$, a set pressure ratio $PR = 0.3$, 0.5 and 0.8, and two rotor speeds, 0 and 7.5 krpm. The hollow square symbols represent the mass flow rate at null rotor speed, whereas the solid triangles denote the mass flow rate at 7.5 krpm shaft speed ($\Omega R = 59$ m/s). At a constant pressure ratio (PR), the mass flow rate increases linearly with an increase in ΔP, and is not a function of rotor speed. Additionally, with or without rotor speed, swirl brakes have little effect on the recorded seal leakage. As in Ref. [1], the mass flow rate uncertainty is $U_M \sim 5\%$.

Figure 10 depicts the measured mass flow rate ($\dot{m}$) and predictions from a bulk-flow model (BFM) tool [11], versus pressure difference (ΔP) for the three test seal configurations operating at PR= 0.3, 0.5 and 0.8, and one rotor speed ($\Omega = 7.5$ krpm). The hollow symbols represent the predictions whereas the solid symbols denote measurements. Triangle, diamond, and circle symbols denote the test data at pressure ratio PR = 0.3, 0.5, and 0.8, respectively. As in Ref. [1], the BFM delivers leakage rates within ~ 4% of measured magnitudes for PR= 0.3, 0.5, and 0.8. In short, the measured leakage validates the predictive model output.

The gas flowing through the seal has an axial velocity component setting the leakage and a circumferential velocity component denoting the swirl; hence, the axial flow Reynolds number $\text{Re}_a = \dot{m}/(\pi D \mu)$ and the circumferential flow Reynolds number $\text{Re}_c = \left(\rho_{out}/\mu\right)\Omega R C_r$. For the entire set of measurements conducted, the flow Reynolds number $\text{Re} = \sqrt{\text{Re}_c^2 + \text{Re}_a^2} > 2,000$ for all inlet pressures thus denoting turbulent flow conditions. For a low PR = 0.3 and 0.5, $\text{Re}_a > \text{Re}_c$; whereas for a high PR =0.8, the leakage is low and $\text{Re}_c > \text{Re}_a$.
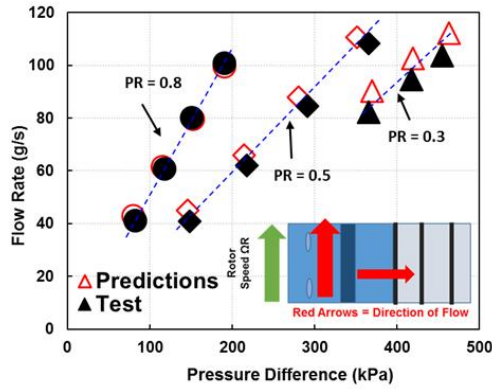

(a) Seal with no swirl brake [1]

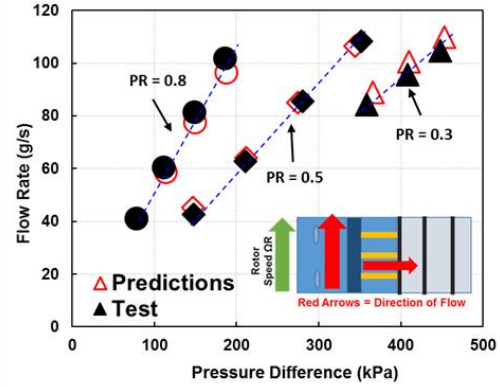(b) Seal with swirl brake, 0° teeth pitch
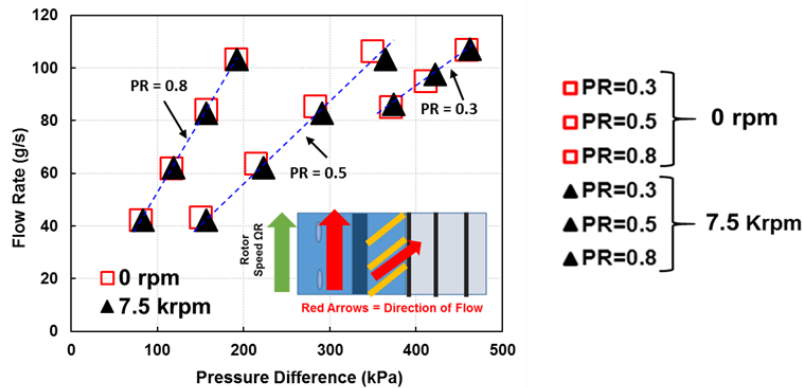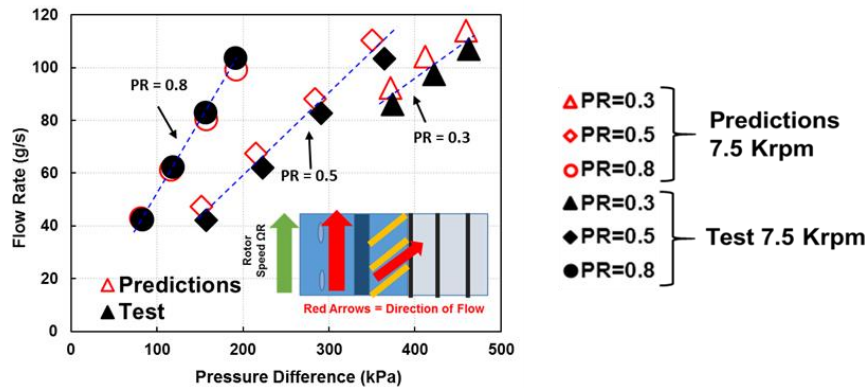
(c) Seal with swirl brake, 40° teeth pitch

Figure 9. Measured mass flow rate versus pressure difference ($P_{in} – P_{out}$) for three test seal configurations: (a) no swirl brake, (b) swirl brake with 0° teeth pitch, and (c) swirl brake with 40° teeth pitch. ILS operates at pressure ratio PR = 0.3, 0.5, 0.8, and two rotor speeds (Ω =0, 7.5 krpm, max $R\Omega$ = 59 m/s).

11

(a) Seal with no swirl brake [1]

(b) Seal with swirl brake, 0° teeth pitch

(c) Seal with swirl brake, 40° teeth pitch

Figure 10. Measured and Bulk Flow Model (BFM) predicted mass flow rate versus pressure difference (P_{in} – P_{out}) for three test seal configurations: (a) no swirl brake, (b) swirl brake with 0° teeth pitch, and (c) swirl brake with 40° teeth pitch. ILS operates at pressure ratio PR = 0.3, 0.5, 0.8, and two rotor speeds (Ω =0, 7.5 krpm, max $R\Omega$ = 59 m/s).

Seal cavity pressures

Figure 11 illustrates the measured cavity pressures (P_i / P_{in}, i = 1, 4) for operation at rotor speed Ω= 7.5 krpm, and various P_{in}, P_{out} for the three seal configurations shown in Figure 7. The square, circle, and triangle symbols represents the seals with (a) no swirl brake teeth, (b) swirl brake with 0° teeth pitch, and (c) swirl brake with 40° teeth pitch in the direction of shaft rotation, respectively. Red, blue, and black symbols denote operation at pressure ratio PR = 0.3, 0.5, and 0.8, respectively. For PR = 0.5 and 0.8, the seals show a linear drop in cavity pressures from the inlet plane to the outlet plane, as evidenced by the solid lines. However, for PR = 0.3 there is a significant change in pressure drop across the last tooth due to a choked flow condition. The findings hereby reported are similar to those stated in Ref. [1].

For the test seal with a swirl brake with 40° teeth pitch, Figure 12 compares the measured vs. BFM predicted cavity pressures (P_i / P_{in}) for operation at rotor speed Ω= 7.5 krpm and various P_{in}, P_{out}. The solid square represents predictions whereas the hollow triangles denote the measurements. Red, blue, and black symbols denote operation at pressure ratio PR = 0.3, 0.5, and 0.8, respectively. As expected, for tests with PR = 0.5 and 0.8, P_i drops linearly; whereas for PR = 0.3, both the measured and BFM results show a significant drop in the fourth cavity toward the exit pressure. The difference between the measured and BFM cavity pressure results is ~5% for tests with PR = 0.5 and 0.8. However, for PR = 0.3, the BFM results are 15% away, with the largest difference occurring in the fourth cavity.
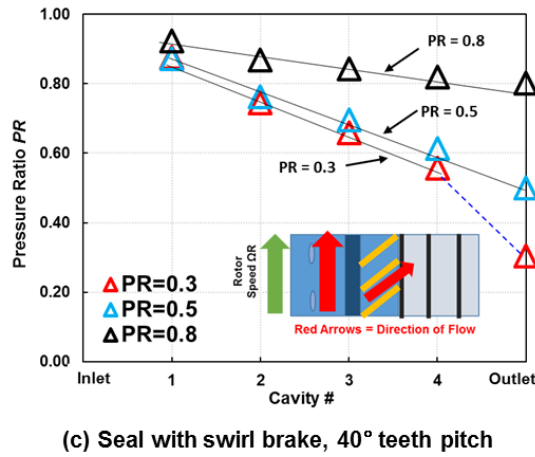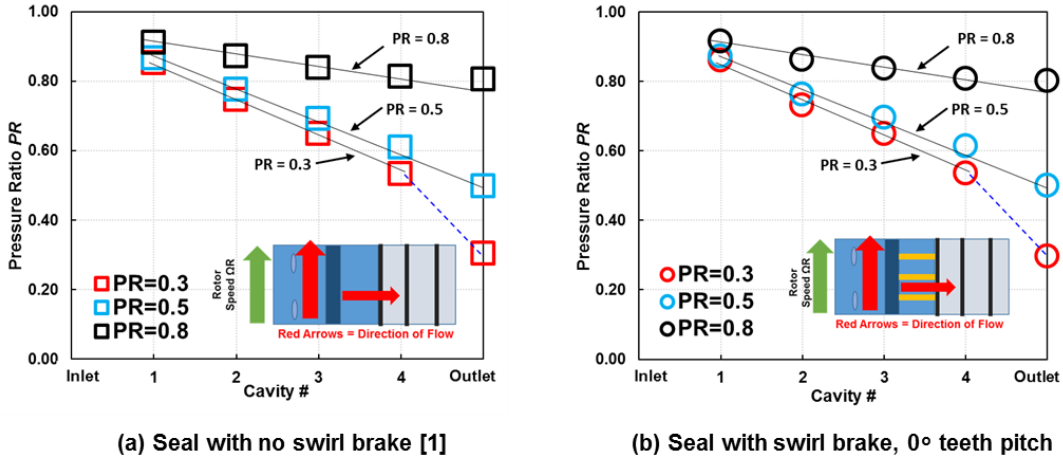
(a) Seal with no swirl brake [1]

(b) Seal with swirl brake, 0° teeth pitch

(c) Seal with swirl brake, 40° teeth pitch

Figure 11. Measured cavity pressure (P_i/P_{in}, i = 1, 2, 3, 4) versus cavity # for three test seal configurations: (a) no swirl brake, (b) swirl brake with 0° teeth pitch, and (c) swirl brake with 40° teeth pitch. ILS operates at pressure ratio PR = 0.3, 0.5, 0.8, and at rotor speed (Ω =7.5 krpm). Inlet pressure P_{in} ranges from 0.29 MPa to 0.98 MPa.
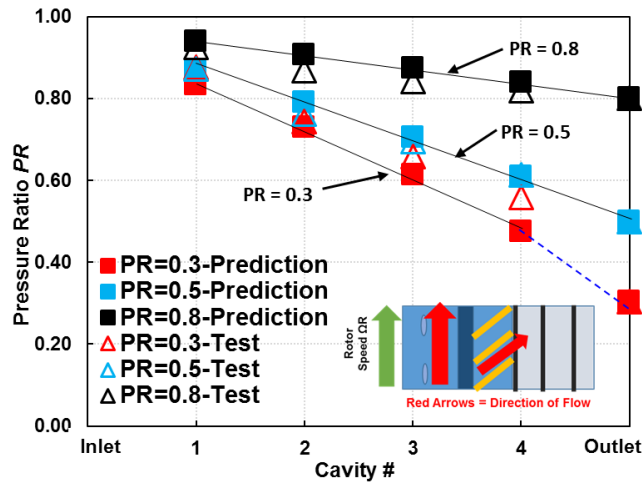

Figure 12. Measured and predicted cavity pressure (P_i/P_{in}, i =1, 2, 3, 4) versus cavity # for test seal with swirl brake with 40° teeth pitch. ILS operates at pressure ratio PR = 0.3, 0.5, 0.8, and at rotor speed (Ω =7.5 krpm, RΩ = 59 m/s). Inlet pressure P_{in} ranges from 0.29 MPa to 0.98 MPa.

13

Modified flow factor and ILS flow loss coefficient

Presently, for the measured leakage results hereby reported, namely those shown in Figure 9 and Figure 10 for the three test seal configurations, Figure 13 depicts the extracted modified flow factor $\bar{\Phi} = \left[\frac{\dot{m}\sqrt{T}}{P_{in} D\sqrt{1-PR^2}} \right]$ vs. inlet pressure (P_{in}) for operation at PR = 0.3, 0.5, 0.8, and rotor speed Ω = 7.5 krpm.

The analysis delivers average $\bar{\Phi} \sim 19.6 \ [kg\sqrt{K}/(MPa \cdot m \cdot s)]$ with standard deviation $\sigma_{\bar{\Phi}} = 0.55$ $[kg\sqrt{K}/(MPa \cdot m \cdot s)]$, just 2.8% of the mean value, for inlet pressure (P_{in}) ranging from 0.29 MPa to 0.98 MPa and pressure ratio PR=0.3 $\rightarrow$ 0.8. The finding is remarkable as the swirl brakes do not affect the flow coefficient $\bar{\Phi}$. The physical measured leakage ($\dot{m}$) shown in Figure 8 already shows this behavior.

Incidentally, leakage measurements for a test ILS with clearance 0.2 mm produces a unique $\bar{\Phi} \sim 12.75$ $[kg\sqrt{K}/(MPa \cdot m \cdot s)]$ [1] for all operating conditions in inlet and exit pressures as well as rotor speed, low and high. Recall the tests seals in [1] did not have swirl brake.
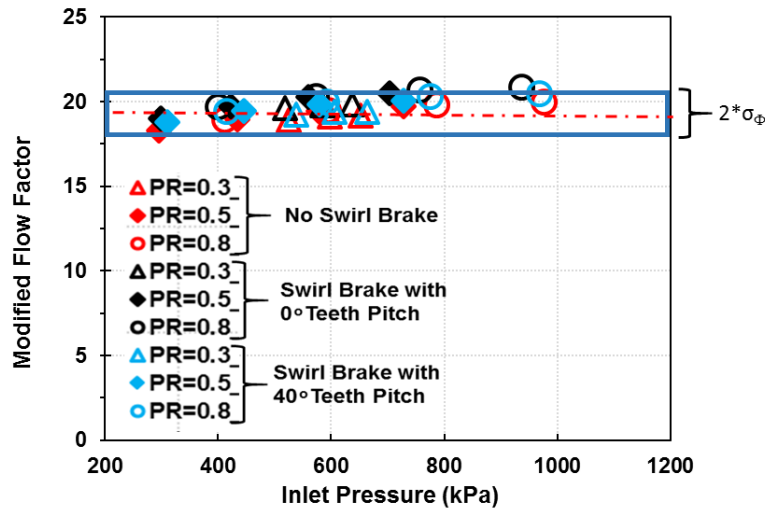

Figure 13. Modified flow factor $\bar{\Phi}$ versus inlet pressure P_{in} for three test seal configurations: (1) no swirl brake teeth, (2) swirl brakes with 0° teeth pitch, and (3) swirl brakes with 40° teeth pitch. ILS operates at pressure ratio PR = 0.3, 0.5, 0.8 and rotor speed Ω =7.5 krpm ($R\Omega$ = 59 m/s). Box width denotes two standard deviations and the dash line is for $\bar{\Phi} \sim 19.6 \ [kg\sqrt{K}/(MPa \cdot m \cdot s)]$.

From Eq. (5), the test seal flow loss coefficient (c_d) equals

$$c_d = \frac{\dot{m}\sqrt{R_g T}}{\pi D C_r P_{in}\sqrt{1-PR^2}} = \bar{\Phi}\frac{\sqrt{R_g}}{\pi C_r} \tag{6}$$

Analysis of the whole set of test results for the three seal configurations delivers $c_d = 0.36 \pm 0.01$, whereas $c_d = 0.37 \pm 0.01$ for the predictions. Notably, San Andrés et al. [1] also obtain for the 0.2 mm clearance ILS a nearly identical $c_d = 0.36 \pm 0.01$ from the measured leakage, and $c_d = 0.35 \pm 0.01$ from the predicted leakage. That is, the flow loss coefficient (c_d) remains relatively constant for the test ILS, irrespective of its clearance (0.2 and 0.3 mm) and whether installed with or without swirl brakes.

CONCLUSION

The paper discussed measurements of leakage and cavity pressures in a test rig hosting interlocking labyrinth seals (ILS) of various configurations. The test section comprises two identical ILSs separated by a central ring. A test ILS has five teeth with a nominal radial clearance C_r=0.3 mm. The central ring has two rows of 14 equally spaced inlet orifices angled at 75° from the radial direction and in the direction of rotor rotation. The mid ring section allows

14

the installation of swirl brakes with engineered configurations. Presently, test results compare the leakage performance of an ILS with a swirl brake with 0° teeth pitch (axial ribs) against another ILS with a swirl brake with ribs angled 40° (direction of rotor spinning), and against a baseline ILS without a swirl brake.

Analysis of the measured leakage and static cavity pressures for operation with inlet pressure P_{in} ranging from 0.29 MPa to 0.98 MPa, pressure ratio $PR = (P_{out}/P_{in}) = 0.3, 0.5, 0.8$, and rotor speed = 7.5 krpm and also a stationary shaft, shows

- For all test conditions (P_{in}, PR, rotor speed), the test ILSs produce the same mass flow rate and cavity pressures irrespective of the swirl brake configuration.

- Rotor surface speed, as large as 59 m/s at 7.5 krpm, shows a negligible effect on the test seals' mass flow rate.

- The mass flow rate for the test ILSs is proportional to the inlet pressure and increases as PR decreases.

- The seal cavity static pressures drop linearly for all inlet pressures (P_{in}) and pressure ratio $PR = 0.5$, and 0.8. For $PR=0.3$, the pressure drop is not linear in the last cavity, on account of the choked flow condition

- The BFM [11] predicted mass flow rate and cavity static pressure predictions are in excellent agreement with the measurements.

- A single flow factor $\bar{\Phi} \sim 19.6$ [$kg\sqrt{K}/(MPa \cdot m \cdot s)$] characterizes the seal mass flow rate for three test seal configurations. Note the found $\bar{\Phi}$ is not a function of inlet pressure, pressure ratio, or shaft speed.

- Further analysis to evaluate a seal effective clearance produces a flow loss coefficient $c_d = 0.36 \pm 0.01$, and which is also valid for another test ILS with radial clearance equal to 0.2 mm [1].

- The ILS with swirl brakes with 40° teeth pitch reduced the inlet gas swirl velocity at the (upstream) central plenum by as much as 30% compared to the swirl speed in the baseline ILS. The effect of swirl brakes on the swirl velocity is largely unknown because the gas swirl velocity in the first cavity was not recorded.

NOMENCLATURE

c_d	Seal loss Coefficient [-]
C_{eff}	$c_d\,C_r$. Seal Effective Clearance [m]
C_r	Seal radial clearance [m]
D	$2R$. Rotor diameter [m]
$\dot{m}$	$\rho_s\,Q$. Mass flow rate through seal [kg/s]
N_T	Teeth Number = 5
N_C	Number of cavities = 4
P_{in}	Inlet Pressure [kPa]
P_{out}	Outlet Pressure [kPa]
P_i	Seal Cavity Pressure ($i = 1, 2 \ldots N_C$) [kPa]
PR	(P_{out}/P_{in}). Pressure Ratio [-]
R_g	Air Gas Constant [J/(kg K)]
R	½ D. Rotor Radius [m]
U_θ	ΩR. Rotor Surface Speed [m/s]
U_{swirl}	Gas inlet swirl velocity in feed chamber [m/s]
V	Fluid axial velocity [m/s]
W_t	Cavity width between teeth tips [mm]
T	Temperature [K]
ρ	$P/(R_g T)$. Gas density [kg/m³]
ϕ	$\dot{m}\sqrt{T}/(D\,P_{in})$. Seal flow factor [$kg\sqrt{K}/(MPa \cdot m \cdot s)$]
$\bar{\Phi}$	$\phi/\sqrt{1-PR^2}$. Seal modified flow factor [$kg\sqrt{K}/(MPa \cdot m \cdot s)$]
μ	Gas absolute viscosity [Pa-s]
Ω	Rotor speed [rad/s]

REFERENCES

[1] San Andrés, L., Wu, T., Barajas-Rivera, J., Zhang, J., and Kawashita, R., 2019, "Leakage and Cavity Pressures in an Interlocking Labyrinth Gas Seal: Measurements vs. Predictions," ASME Paper No. GT2019-91507 (Accepted for journal publication).

[2] Childs, D. W., 1993, Turbomachinery Rotordynamics: Phenomena, Modeling, and Analysis, Chap.5, "Rotordynamic Models for Annular Gas Seals," John Wiley & Sons, pp. 209-306.

[3] Benckert, H., and Wachter, J., 1980, "Flow Induced Spring Coefficients of Labyrinth Seals for Application in Rotor Dynamics," Proc. of a Workshop on Rotordynamic Instability Problems in High-Performance Turbomachinery, Texas A&M University, College Station, TX, NASA Accession No. 80N29717, pp. 189-212.

[4] Childs, D. W., Elrod, D. A., and Hale, K., 1988, "Rotordynamic Coefficient and Leakage Test Results for Interlock and Tooth-on-Stator Labyrinth Seals," ASME Paper 88-GT-87.

[5] Paolillo, R., Moore, S., Cloud, D., and Glahn, J. A., 2007, "Impact of Rotational Speed on the Discharge Characteristic of Stepped Labyrinth Seals," ASME Paper No. GT2007-28248.

[6] Bozzi, L., D'Angelo, E., Facchini, B., Micio, M., and Da Soghe, R., 2011, "Experimental Investigation on Leakage Losses and Heat Transfer in a Non-Conventional Labyrinth Seal," ASME Paper No. GT2011-46362.

[7] Vannini, G., Cioncolini, S., Del Vescovo, G., and Rovini, M., 2014, "Labyrinth Seal and Pocket Damper Seal High Pressure Rotordynamic Test Data," ASME J Eng Gas Turb Power, **136**(2), pp. 022501.

[8] Childs, D. W., Mclean, J. E., Jr., Zhang, M., and Arthur, S. P., 2016, "Rotordynamic Performance of a Negative-Swirl Brake for a Tooth-on-Stator Labyrinth Seal," ASME J Eng Gas Turb Power, **138**(6), pp. 062505.

[9] Gary, K., Childs, D. W., and Ramirez, M. A., 2018, "Measurements of the Leakage and Rotordynamic Performance of Interlocking Labyrinth Seals," ASME Paper GT2018-75885.

[10] Neumann, K., 1964, "Zur Frage der Verwendung von Durchblickdichtungen im Dampfturbinenbau," Maschinenbautechnik, **13**(4), pp. 188-195.

[11] Thorat, M., and Childs, D., 2010, "Predicted Rotordynamic Behavior of a Labyrinth Seal as Rotor Surface Speed Approaches Mach 1," ASME J. Eng. Gas Turbines Power, **132**(11), pp. 112504.

[12] Delgado, I., and Proctor, M., 2006, "Continued Investigation of Leakage and Power Loss Test Results for Competing Turbine Engine Seals," 42nd AIAA/ASME/SAE/ASEE Joint Propulsion Conference & Exhibit, Sacramento, California, July 9-12. Paper number: AIAA–2006–4754.